

Thin-film $\text{YBa}_2\text{Cu}_3\text{O}_{7-x}$ direct current SQUIDs with Josephson junctions made by direct electron beam writing

B. Nadgorny,^{a)} S. Shokhor, and M. Gurvitch

Department of Physics, State University of New York at Stony Brook, Stony Brook, New York 11794

S. Y. Hou and Julia M. Phillips^{b)}

AT&T Bell Laboratories, Murray Hill, New Jersey 07974

(Received 17 June 1996; accepted for publication 15 August 1996)

We have investigated dc superconducting quantum interference devices (SQUIDs) with loop areas 8 and 64 μm^2 made by direct electron beam writing in $\text{YBa}_2\text{Cu}_3\text{O}_{7-x}$ films with thickness 25 and 50 nm. The SQUIDs have maximum peak-to-peak voltage modulation of about 20 μV , which corresponds to the transfer factor $dV/d\Phi_0 \sim 50\text{--}60 \mu\text{V}/\Phi_0$ at 30–40 K. By measuring the mutual inductance of the SQUID signal line as a function of temperature and comparing the data with the numerical calculations and the two-fluid model, we extracted the values of the London penetration depth for $\text{YBa}_2\text{Cu}_3\text{O}_{7-x}$ thin films. © 1996 American Institute of Physics. [S0003-6951(96)03443-2]

Over the last few years significant progress has been made in the improvement of the characteristics of HTS Josephson junctions and superconducting quantum interference devices (SQUIDs), based on bicrystal, step edge, and SNS structures. A typical transfer factor of the HTS dc SQUIDs is of the order of 20–30 $\mu\text{V}/\Phi_0$ (Φ_0 —magnetic flux quantum) at 77 K, which is suitable for most applications, with a recently reported¹ value of 100 $\mu\text{V}/\Phi_0$ for highly resistive bicrystal junctions. The noise level of the best HTS SQUIDs is approaching that of commercially available low- T_c SQUIDs.^{1,2}

Progress in the development of digital multijunction HTS circuits, however, has been far less impressive. To a large extent this is due to problems of reproducibility and uniformity in the existing junction technologies. Another serious problem is related to the circuit design restrictions imposed by most of these technologies, which require all the junctions to be placed along one line (e.g., grain boundary) or several parallel lines. In practice, these restrictions may lead to large inductances of the circuits that make it rather difficult to use these junctions in the plane geometry for digital circuits, e.g., for RSFQ logic.

The direct e-beam writing (DEW) technique developed at Stony Brook and Cambridge^{3–5} for HTS thin films has certain advantages, such as simplicity and good reproducibility as well as flexibility in terms of circuit layout, which makes it, perhaps, best suited for the investigation of multijunction circuits. In our recent letter, we demonstrated a 14-junction HTS RS flip-flop operating at $T \sim 30$ K, made by direct e-beam writing.⁶ The heart of practically any RSFQ circuit is a double-junction interferometer (dc SQUID). The constraints on the SQUID parameters, such as inductance, critical current, and normal resistance have been well established⁷ and can be used for 77 K SQUID applications with some modifications.⁸ The SQUID in a RSFQ circuit should ideally have two stable states (one with zero flux and another with one flux quantum),⁹ resulting in the condition for $\beta_L = LI_c/\Phi_0 = 1\text{--}3$, where L and I_c are the inductance

and critical current of the SQUID, respectively. Therefore, the relation between I_c and L is quite similar to that for magnetometric SQUID applications.⁷

In order to minimize the influence of thermal fluctuations¹⁰ for analog SQUIDs, I_c should be 5–6 times larger than the thermal current $I_{\text{th}} = 2\pi k_B T/\Phi_0$, where T is the operating temperature. This requires critical currents no less than approximately 8 μA at 30 K and 20 μA at 77 K. The critical current I_c in the case of RSFQ circuits is restricted from below by the thermally induced error rates. Rigorous analysis is more complicated in this case and depends on the actual circuit type. Some estimates will be given elsewhere; we only note here that the requirements for I_c are in general more stringent (I_c should be several times higher) for digital than analog applications.

The aim of this work is to describe the properties of DEW-made SQUIDs with small loops on $\text{YBa}_2\text{Cu}_3\text{O}_{7-x}$ films, and also to obtain some insight into the properties of DEW-made junctions that are still not completely understood. Because of the limitations on I_c discussed above, small loops are needed to reduce the inductance in RSFQ circuits.⁹ The kinetic inductance of the film L_k may constitute a large part of the total inductance L_T . Since in the film thickness region $d \leq \lambda_L$, the kinetic inductance is approximately inversely proportional to the film thickness d , it is also desirable to use thicker film. (The voltage modulation and, therefore, the operating speed of the circuit, defined by the product of $I_c R_n$, for $d \leq \lambda_L$ is almost independent of the film thickness.) The junction preparation was described in some detail in Ref. 4. After a microbridge is made using standard optical lithography and wet etch, a focused electron beam is scanned across the microbridge to produce a narrow line of damage, which serves as a weak link. The length of the damaged region in the direction of the transport current depends on the electron-beam broadening, which in turn is smaller for thinner films. For our electron-beam energy (120 keV), the film thickness should be less than 100 nm to ensure high quality junctions. Together with the requirements for the kinetic inductance, this defines the limitations on the films' thickness we can use; for higher energy electron irradiation thicker films can be used.⁵ While we worked mostly

^{a)}Present address: Naval Research Laboratory, Washington, DC 20375.

^{b)}Present address: Sandia National Laboratories, Albuquerque, NM 87185.

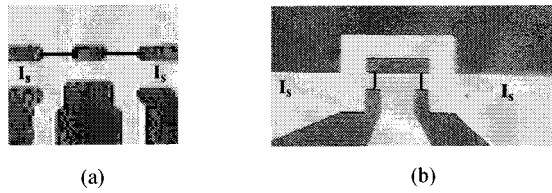


FIG. 1. Layouts for the $8 \mu\text{m}^2$ and (a) $64 \mu\text{m}^2$ (b) size loop interferometers. Hand-drawn lines indicate locations of the Josephson junctions.

with 25 and 50 nm thick $\text{YBa}_2\text{Cu}_3\text{O}_{7-x}$ films grown by the BaF_2 process¹¹ on LaAlO_3 , we obtained similar results on laser ablated film up to 100 nm thick, and on different substrates, in particular, on Si with a YSZ buffer layer. Figure 1 shows layouts for the two types of SQUIDs we describe here: with loop area $8 \mu\text{m}^2$ (a), and $64 \mu\text{m}^2$ (b). The following features of our junctions are important for the discussion of the operation of the SQUIDs.

(1) The effective critical temperature T_{c0} of the junction (which is defined as the onset of the critical current of $1 \mu\text{A}$, see below) can be varied from 87 K down to 4.2 K depending on the irradiation dose.⁴ Critical temperature T_c of the rest of the film remains unchanged.

(2) At $T_{c0} < T < T_c$ resistance of the damaged region decreases monotonically with temperature, which we attributed to narrowing of the normal part of the damaged region as the temperature decreases. At $T = T_{c0}$, when the effective length of the region reaches a few hundred angstroms, critical current becomes observable (see inset in Fig. 2).

Within a certain temperature range $T_{c0}^* < T < T_{c0}$ the junction is a Josephson weak link. The $I-V$ characteristics of the junction are close to the RSJ shape at small currents and to parabolic shape at larger currents: $V = A(T)I^2 + R_n^*(T)I + B(T)$, where $A(T)$, $R_n^*(T)$, and $B(T)$ are some temperature dependent coefficients. Normal resistance of the junction R_n is then defined as a linear term R_n^* of the fitting curve, whereas a quadratic term can be associated with the vortex motion and $B(T)$ with the excess current. R_n^* monotonically decreases with temperature and reaches zero at T_{c0}^* . Below this temperature, the $I-V$ characteristics of the

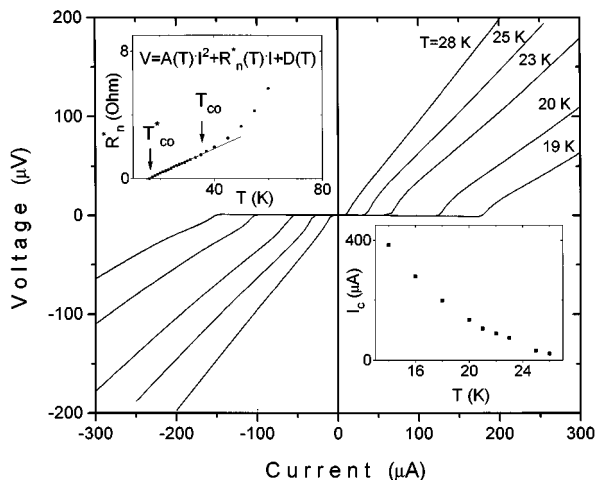


FIG. 2. Current-voltage characteristics of the $8 \mu\text{m}^2$ loop SQUID with $T_{c0} = 34 \text{ K}$ at different temperatures. Insets show the temperature dependence of R_n^* (upper left) and I_c (lower right).

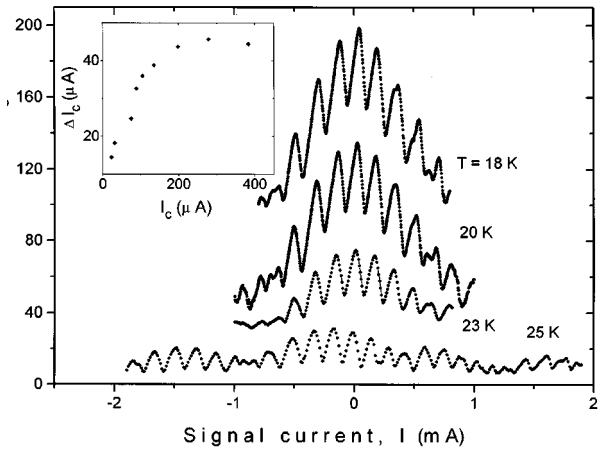


FIG. 3. Modulation of the critical current of the $8 \mu\text{m}^2$ loop SQUID vs signal current; inset contains the dependence of the maximum amplitude of critical current modulation vs critical current.

junction gradually transform from an RSJ-type to a flux-flow type with $V \sim I^2$. This may imply that at T_{c0}^* the damaged region becomes superconducting.⁴ Typical $I-V$ curves at different temperatures for the SQUID with $T_{c0} = 34 \text{ K}$ are shown in Fig. 2, along with the temperature dependencies of I_c and R_n^* .

Figure 3 demonstrates the critical current modulation for an $8 \mu\text{m}^2$ dc SQUID, shown in Fig. 1(a), at different temperatures. Because of the small size of the loop, the period of SQUID modulation is comparable to the period of the junction modulation itself, which is seen in Fig. 3 for the bottom curve. The mutual inductance L_m between the signal current line [I_s in Fig. 1(a)] and the SQUID loop can be calculated from the period of modulation of I_c vs I_s using the formula $L_m = \Phi_0 / \Delta I_s$. At $T = 34 \text{ K}$ it gives $L_m \sim 12 \text{ pH}$. The total inductance L_T of the SQUID can be estimated from the maximum modulation amplitude ΔI_c of the critical current I_c according to the formula $L_T = \Phi_0 / \Delta I_c$ at $L I_c / \Phi_0 \gg 1$, where ΔI_c saturates.⁷ The inset shows ΔI_c as a function of I_c with a saturation value of $\Delta I_c \sim 50 \mu\text{A}$. This corresponds to a total inductance of 40 pH. Numerical modeling using calculations of the inductance matrices for superconductive film based on the exact solutions of the London equations¹² with λ_L as a free parameter allows us to obtain both L_m and L_T , which are in good agreement with the experimental results. From the same calculations we see that the geometrical inductance is only a small part of L_T ($L_g = 5.5 \text{ pH}$).

Since we can change the effective temperature of the junctions T_{c0} by annealing them at relatively low temperature ($T = 330 \text{ K}$) we can select the operating temperature of our SQUIDs within a wide temperature range. By measuring the temperature dependence $L_m(T) \sim \lambda_L^2(T)/d$ for thin films, we can study the temperature dependence of λ_L . Figure 4 shows the results of such measurements for the $64 \mu\text{m}^2$ loop SQUIDs [see Fig. 1(b)] made from 25 and 50 nm films. It can be seen that for 25 and 50 nm films the inductance scales nicely with the thickness of the film, which implies that the kinetic inductance is inversely proportional to the film thickness with a very good accuracy in this thickness range. $L_m(T)$ can be fitted by the empirical Gorter-Casimir two-fluid model (solid line) in a wide temperature range. Deviation of the inductance from the two fluid formula (which

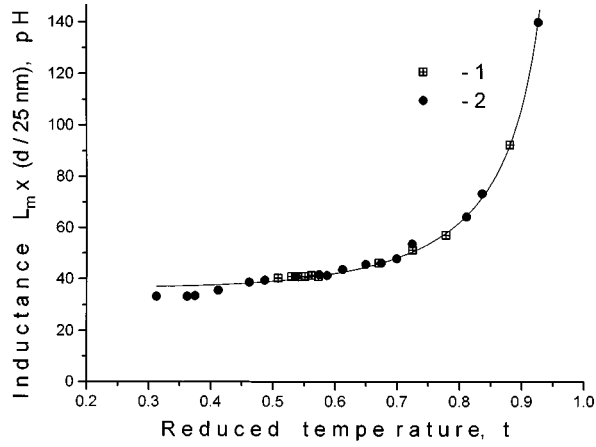


FIG. 4. Reduced temperature dependence of the mutual inductance L_m for the $64 \mu\text{m}^2$ loop SQUID with the film thickness of 25 nm (data set 1) and 50 nm (data set 2). The solid line is a fit by the function $L_m(T) = L_m(0)/(1 - t^4)$.

usually describes conventional (BCS) pairing rather well seen at low temperatures is often interpreted within the framework of a d -wave pairing mechanism,¹³ however, the preliminary data reported in this letter does not allow us to draw definite conclusions. Extrapolation of this dependence to $T=0$ and comparison with the numerically calculated value gives $\lambda_L(0) \sim 0.35 \mu\text{m}$, which is not uncommon for thin films, particularly for those made by the BaF₂ process used in our experiment.¹⁴ As can be seen from Fig. 4, it is preferable for the SQUIDs to operate at temperatures $T < 0.6T_c$ (below 55 K for YBa₂Cu₃O_{7-x}), so that the inductance of the film is the smallest and almost temperature independent. Most of our small loop SQUIDs were fabricated to obtain $T_{co} < 50$ K in order to be able to work at lower temperatures.

Finally, we present the results on SQUID voltage modulation. Figure 5(a) shows maximum peak-to-peak modulation of the $8 \mu\text{m}^2$ (a) and $64 \mu\text{m}^2$ (b) loop SQUIDs. Figure 5(b) gives the temperature dependence of ΔV_{max} for $8 \mu\text{m}^2$ SQUID. The experimental data are compared with the estimates obtained from the formula derived in Ref. 8, which takes into account the thermal noise,

$$\Delta V_{\text{max}}(T) = \frac{4I_c(T)R_n^*(T)}{\pi(1 + \beta_L(T))} (1 - 3.57\sqrt{k_B L(T)T/\Phi_0}),$$

where $I_c(T)$ and $R_n^*(T)$ are the experimental values. Agreement is quite good at small critical currents, where this formula is applicable. It can be seen that instead of saturation, as in other types of SQUIDs, ΔV_{max} reaches its maximum at some temperature and then starts to decrease. This decrease in ΔV_{max} is connected to the dominant decrease of $R_n^*(T)$ in the expression for ΔV_{max} .

To conclude, we have made and studied double-junction interferometers fabricated using the direct electron-beam writing technique. This simple technology allows us to make small-loop SQUIDs with adequate current and voltage modulation for use in digital circuits of the RSFQ family.⁶ We have also studied the kinetic inductance and the London penetration depth in YBa₂Cu₃O_{7-x} thin films.

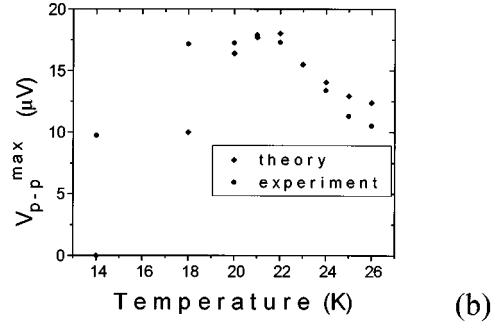
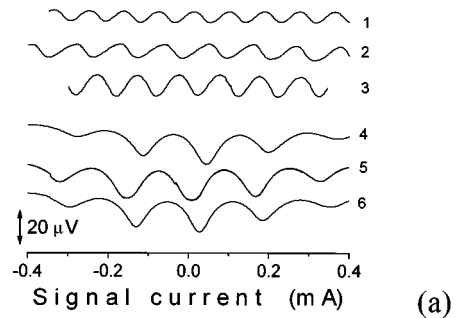


FIG. 5. Maximum peak-to-peak voltage modulation at different operating temperatures for the $8 \mu\text{m}^2$ (curves 1–3) and $64 \mu\text{m}^2$ (curves 4–6) size loop SQUIDs, (b) experimental and theoretical (Ref. 8) temperature dependence of the maximum peak-to-peak voltage modulation.

The authors would like to thank A. King and J. Lukens for the use of their laboratory facilities, D. Rudman, R. Ono, and P. Rosenthal for providing some of the films, Yu. Polyakov for technical help with some of the measurements, and M. Khapaev for providing a program for numerical modeling. The authors gratefully acknowledge numerous discussions and valuable advice from K. Likharev. This work was supported by ONR Grant No. N0001494IG026.

- ¹L. P. Lee, M. Teepe, V. Vinetskiy, R. Cantor, and S. Colclough, *Appl. Phys. Lett.* **66**, 3059 (1995).
- ²Y. Zhang, M. Muck, K. Hermann, J. Schubert, W. Zander, A. I. Braginski, and C. Heiden, *IEEE Trans. Appl. Supercond.* **3**, 2465 (1993); D. Koelle, A. H. Michlich, E. Ludwig, E. Dantsker, D. T. Nemeth, J. Clarke, W. Ruby, and K. Chan, *Appl. Phys. Lett.* **63**, 3630 (1993); M. Faley, U. Poppe, C. L. Lia, U. Dahne, Yu. Goncharov, N. Klein, U. Urban, V. N. Glyantsev, G. Kunkel, and M. Siegel, *IEEE Trans. Appl. Supercond.* **5**, 2608 (1995).
- ³S. K. Tolpygo *et al.* *Physica C* **209**, 211 (1993); S. K. Tolpygo, S. Shokhor, B. Nadgorny, J. Y. Lin, M. Gurvitch, S. Y. Hou, and J. M. Phillips, *Appl. Phys. Lett.* **63**, 904 (1993).
- ⁴S. K. Tolpygo, S. Shokhor, B. Nadgorny, J.-Y. Lin, M. Gurvitch, S. Y. Hou, and J. M. Phillips, *IEEE Trans. Appl. Supercond.* **5**, 2521 (1995).
- ⁵A. J. Pauza, A. M. Campbell, D. F. Moore, R. E. Somekh, and A. N. Broers, *IEEE Trans. Appl. Supercond.* **3**, 2405 (1993).
- ⁶S. Shokhor, B. Nadgorny, M. Gurvitch, V. Semenov, Yu. Polyakov, K. Likharev, S. Hou, and J. M. Phillips, *Appl. Phys. Lett.* **67**, 2869 (1995).
- ⁷C. D. Tesche and J. Clarke, *J. Low Temp. Phys.* **29**, 310 (1977).
- ⁸K. Enpuku, Y. Shimomura, and T. Kisu, *J. Appl. Phys.* **73**, 2779 (1993).
- ⁹K. K. Likharev and V. K. Semenov, *IEEE Trans. Appl. Supercond.* **1**, 3 (1991).
- ¹⁰V. Ambegaokar and B. I. Halperin, *Phys. Rev. Lett.* **22**, 1364 (1969).
- ¹¹M. P. Siegal, S. Y. Hou, J. M. Phillips, T. D. Tiefel, and J. H. Marshall, *J. Mater. Res.* **7**, 2658 (1992).
- ¹²M. Khapaev (unpublished).
- ¹³L. S. Borkowski and P. J. Hirschfeld, *Phys. Rev. B* **49**, 15 404 (1994).
- ¹⁴A. F. Hebard, A. T. Fiory, M. P. Siegal, J. M. Phillips, and R. C. Haddon, *Phys. Rev. B* **44**, 9753 (1991).